*Journal of Undergraduate Chemistry Research,* **2023**, 22(4), 78

# CHANGING THE ONSET OF THE DISORDER-TO-ORDER TRANSITION AND INCREASING THE DENSITY OF DEFECT SITES IN BIPHENYL ADLAYER ON $Al_2O_3$

Issac Z. Song*, Samie T. Watanabe* and A.M. Nishimura†

Department of Chemistry, Westmont College, Santa Barbara, CA 93108

**Abstract**

**When biphenyl was vapor deposited on a cryogenically cooled $Al_2O_3$ surface at 120 K, the adlayer was amorphous. Temperature programmed desorption (TPD) experiments showed a disorder-to-order transition at 158 K, that was characterized by a red-shift and a lower fluorescence intensity. If an underlayer of methanol or ethanol was deposited while biphenyl was deposited on top as an overlayer, the amorphous adlayer of biphenyl underwent the ordering transition at a lower temperature. Since aliphatic alcohols desorb at increasing temperatures with increasing carbon chain, the temperature at which the ordering transition occurred in biphenyl, and in other organic solids, could be controlled by proper choice of alcohol. Subsequent to the ordering transition, underlayers of molecules of comparable size to biphenyl, such as cyclic alkanes, were found to cause defects that resulted in an increase in the fluorescence intensity. When both alcohol and cyclic alkanes were used as underlayers, the intensity of the fluorescence subsequent to the ordering transition was substantially muted. Linear alkanes were also used as underlayers to biphenyl, and their effect in increasing the density of defect sites were even more than with cyclic alkanes.**

†Corresponding author: nishimu@westmont.edu *Undergraduate researchers and co-authors
Keywords: biphenyl, methanol, ethanol, cyclohexane, cycloheptane, cyclodecane, $H_2O$, *n*-hexane, *n*-heptane, *n*-octane, *n*-decane, desorption, temperature programmed desorption, TPD
Submitted: June 30, 2023 Accepted: August 16, 2023 Published: August 21, 2023

## Introduction

Biphenyl in the solid phase is an interesting molecule because the dihedral angle is sensitive to its molecular environment.[1-4] For example, upon vapor deposition onto a cryogenically cooled surface of $Al_2O_3$ at 120 K, the adlayer is amorphous with a dihedral angle of about 48º based on the fluorescence $\lambda_{max}$.[5] The disorder-to-order transition occurred at about 158 K with a substantial decrease in the fluorescence intensity due to the emergence of non-radiative pathways in the adlayer molecules.[3-5] Based on $\lambda_{max}$, the dihedral angle of the ordered adlayer was approximately 8º and desorption occurred 227 K.[3-5] This variation in the conformer makes biphenyl a sensor to subtle changes in its environment as the temperature is ramped in a TPD experiment.

In this paper, the effect of different underlayers on the disorder-to-order transition and the ordered state in biphenyl was investigated. Previous studies had shown that underlayers of alkane and cycloalkanes affected the disorder-to-order transition in naphthalenes.[6] and biphenyl.[7-8] At that time, the form of biphenyl upon vapor deposition on $Al_2O_3$ as well and the effect of underlayer molecules on the disorder-to-order transition were not well understood.[7-8] In this paper, a more complete explanation of the effect of underlayer of alcohols and cyclic alkanes is given. Specifically, how these moieties serve to induce the disorder-to-order transition and how they cause traps in the ordered form of biphenyl on $Al_2O_3$. Some years ago, the nucleation-crystallization kinetics[9] of phenanthrene,[10] benzophenone,[11] naphthalene,[11] and cycloalkanone[12] were studied in which the Johnson-Mehl-Avrami-Kolmogorov (JMAK)[9] equation was used to model the disorder-to-order transition. Herein, the JMAK equation was applied to simulate the disorder-to-order transition in biphenyl. Finally, *n*-alkanes were used as underlayers and like the cycloalkanes, *n*-alkanes served in increase the density of defect sites, but in much larger quantity.

## Experimental Methods

All of the compounds that were used in this study were purchased from commercial sources (Sigma-Aldrich, St. Louis, MO). These were placed in separate sample holders and outgassed. Deposition was accomplished from the vapor through any one of three adjustable leak valves from which different compounds can be vapor deposited onto the $Al_2O_3$ substrate.

Details of the experimental set up have been previously published[13-14] and only a brief summary is given here. A LabVIEW (National Instruments, Austin, TX) program was written in-house that takes the complete spectra from the Ocean Optics USB4000 spectrometer (Ocean Optics, Dunedin, FL) continuously and stored in real time during the TPD experiment. The program simultaneously monitored the surface temperature of the $Al_2O_3$ crystal, and via a PID (proportional-integral-derivative) feedback algorithm, linearly incremented the temperature of the $Al_2O_3$ crystal in the TPD experiments at 2 K/s. In addition, the program monitored a residual gas analyzer to determine at what temperature and the quantities of the adsorbates desorbed from the $Al_2O_3$ surface.

Manipulation of the array of spectra as a function of temperature by a MATLAB (Mathworks, Natick, MA) template yielded the wavelength-resolved TPD that are shown in the figures. A peak-picking routine was used to determine $\lambda_{max}$. Mass spectral analysis was accomplished with Excel.

The activation energy for desorption, $E_a$, was calculated by Redhead analysis in which a first-order desorption kinetics as described by King was assumed and was based on the mass spectral peak desorption temperature, $T_p$.[15-17] The uncertainties in the desorption temperatures were ± 1% and the propagated error in the activation energies were ± 1%.

The surface coverages were calculated by calibrating the integrated mass spectral peak recorded from the residual gas anlayzer with an optical interference experiment. The interference experiment yielded accurate rate of deposition, and is described in detail elsewhere[13-14], and is briefly summarized. A laser beam that was impinging on the $Al_2O_3$ surface upon which vapor deposition was being conducted split at the vacuum-adlayer interface; part of the beam was reflected at the interface while the other was refracted in the adlayer and then was reflected at the adlayer-$Al_2O_3$ interface. As the vapor deposition continued and the adlayer thickness increased, the reflected and refracted beams interfered as the pathlength of the refracted beam increased with coverage. Shown in Figure 1 is a representative inteference signal for ethanol, one of the adsorbates in this study. One complete cycle of the interference signal represent roughly one wavelength of adlayer thickness per period. Molecular dimension of a monolayer (ML) was estimated from the density of the compound. The total time of the vapor deposition was related to the integral of the residual gas analyzer signal and a conversion factor was determined to be used in subsequent experiments for deposition of that molecular adalyer in MLs. The surface coverages are given as Θ in ML with an error of ± 30%.

For surface coverages in the multilayer regime, multi-dimensional nucleation and crystal growth is expected at the disorder-to-order transition. In order to model the disorder-to-order transition in biphenyl as a nucleation-crystallization process, the JMAK or simply, Avrami[9] model was used. In the simplest form, the Avrami equation is.[9]

$$I(t) = e^{-kt^n}$$

where I(t) is the time dependent fluorescence intensity at the disorder-to-order transition that is converted to fraction of the disordered state at the transition, k is related to the rate with which crystallization occurs and is in part, a function of the density of nucleation sites, t is time in s and n is the dimensionless Avrami exponent that yields the dimensionality of the nucleation-crystallization process. The unit for k is the inverse of time rised to the $n^{th}$ power. This expression was made to fit the wavelength-resolved TPD data at the disorder-to-order transition using algorithms provided by SciPy and automated with Python in which the parameters were controlled by user interface.

## Results and Discussion

*Multilayer biphenyl*

Shown in Figure 2 is the wavelength-resolved TPD of biphenyl. The fluorescence of the amorphous adlayer had a $\lambda_{max}$ ~ 315 nm. $T_p$ for biphenyl was 227 K and $E_a$ was calculated to be 58.9 kJ/mol[15-17]. From the $\lambda_{max}$, the torsional angle has been estimated at 48º.[5] The onset of the disorder-to-order transition occurred at about 152 K and the transition is complete at 166 K, with a mid-value at 158 K. The molecular fluorescence had a $\lambda_{max}$ at 337 nm (Cf. Fig. 2, inset). From this $\lambda_{max}$, the torsional angle can be estimated to be 8º.[5]

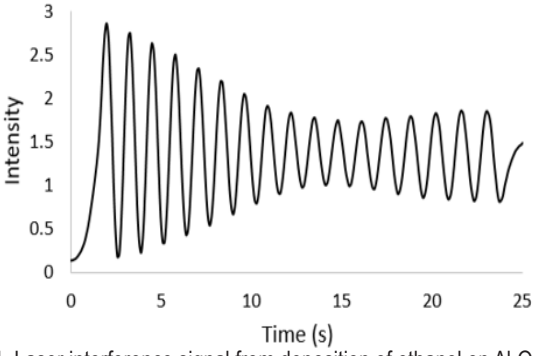


**Figure 1.** Laser interference signal from deposition of ethanol on $Al_2O_3$.

The Avrami nucleation-crystallization analysis showed that n = 4.4 ± 0.4 (with k = 0.1 ± 0.1). This n could be interpreted to mean that crystallization occurred in all three dimensions in addition to another partial degree of freedom attributable to random nucleation.[6-10] The rapid disorder-to-order transition is reflected in the relatively large k value.[6-10]

In order to assign a physical interpretation to n, it should be < 5.[9-12] Since all subsequent Avrami analysis indicated smaller n values, the scan rate used in the TPD experiments was faster than kinetic rates for the other systems.

*Ethanol-Biphenyl Bilayer*

The peak desorption temperature of ethanol was 148 K.

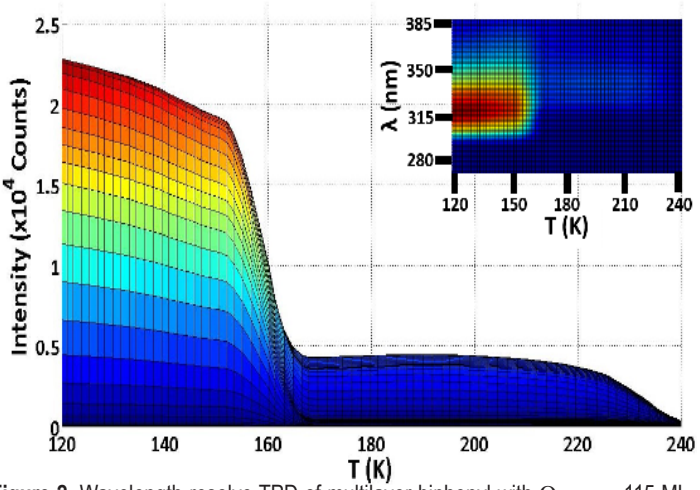


**Figure 2**. Wavelength-resolve TPD of multilayer biphenyl with $\Theta_{biphenyl}$ = 115 ML. Note the disorder-to-order transition that occurs at about 158 K with a concomitant red-shift in $\lambda_{max}$ and decrease in fluorescence intensity to about 20% of the initial intensity. Inset: top view.

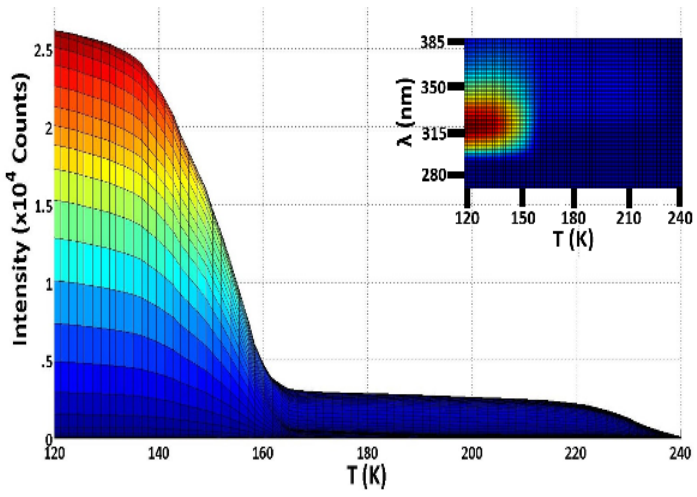


**Figure 3**. Wavelength-resolve TPD of ethanol-biphenyl bilayer with $\Theta_{ethanol}$ = 1 ML, $\Theta_{biphenyl}$ = 101 ML. Note the disorder-to-order transition that occurs at about 144 K with a decrease in fluorescence intensity to about 10% of the initial intensity. Inset: top view.

First-order desorption kinetics was assumed and $E_a$ was calculated to be 37.8 kJ/mol[15-17]. In Figure 3, the wavelength-resolved TPD of a bilayer of ethanol deposited first and biphenyl on top is shown.

For the ethanol-biphenyl bilayer, the onset of the disorder-to-order transition occurred at 136 K, and completed at 158 K, with a mid-value at 150 K. Although the fluorescence intensity after the disorder-to-order transition can vary due to the random nature of the process, the decrease to about 10% can be attributed to the higher degree of ordering than the multilayer. Additionally the disorder-to-order transition of the bilayer occurred at an lower temperature by about 14 K relative to the multilayer. This supports the postulate that ethanol induces ordering in the biphenyl adlayer.

The Avrami model for the nucleation-crystallization process showed a n value of 2.6 ± 1.2 (with k = 0.04 ± 0.03). The n value would suggest that crystallization was 2-dimensional, and reflected the dimensionality of the interface with some degree of randomness of the nucleation sites caused by ethanol. The smaller k value compared to multilayer biphenyl would suggest that the ethanol, as a source of nucleation, was not as effective as biphenyl itself. Note that a smaller k is reflected in longer duration of the disorder-to-transition (22 K, compared to 14 K for multilayer biphenyl). Note that, since the ramp rate was 2 K/s, the duration in time and temperature were related.

In order for an agent to serve as a source of nucleation, an aggregate with a critical radius upon which a crystal of biphenyl can form is required. The size of the ethanol assemblage must be comparable to or, even better, larger than biphenyl itself. Evidence for large molecular cluster formation came from what was loosely termed 'hold down' effect, which was the temperature difference in $T_p$s for the multilayer versus when that molecule is an underlayer to biphenyl. For ethanol, the hold down was an average of 11 ± 3 K with about 100 ML of biphenyl as overlayer. Such a large hold down effect is evidence of hydrogen bonded aggregation, perhaps in the form of micelles in which the cluster size is comparable to or even larger than biphenyl. It should be noted that when the hold down effect was investigated for $H_2O$ as the underlayer to biphenyl, the hold down effect was 72.9 K and is shown in Figure S-1, and was the largest observed.

*Methanol-Biphenyl Bilayer*

Multilayer methanol has a $T_p$ of 139 K and $E_a$ was calculated to be 35.6 kJ/mol. For the bilayer, the disorder-to-order transition temperature was almost identical to that for ethanol as the underlayer with the onset at 134 K and ending at 159 K, and the mid-point occured at 144 K. (Cf. Figure 4). The extent to which methanol ordered the biphenyl adlayer was about the same as with ethanol. Analysis of the nucleation-crystallization kinetics at the disorder-to-order transition gave the best fit with n = 3.1 ± 0.3 (with k = 0.0008 ± 0.0006 and the duration of the transition was 25 K). The hold down effect was about 11 ± 5 K which was identical to that of ethanol and therefore, clustering can be assumed here as well.

The fact that the disorder-to-order transition temperature and Avrami parameters were constant with the alcohol on top or on the bottom (either side of biphenyl adlayer) in the bilayer was another supporting evidence that this was a nucleation-crystallization mechanism that was causing the disorder-to-order transition in biphenyl.

*Cyclohexane-Biphenyl Bilayer*

A more complete set of data for cyclohexane-biphenyl bilayer experiments has been published elsewhere,[18] and only a brief summary is given here. Cyclohexane desorbed at 138 K, and if first-order desorption kinetics can be assumed, activation energy for desorption was calculated as 35.2 kJ/mol. Similar to the alcohols, $T_p$ for cyclohexane was lower than the disorder-to-order transition of biphenyl. In the bilayer, the mid-point temperature of the disorder-to-order transition was 148 K.(Cf. Figure 5). The Avrami kinetics analysis yielded n value of 4.0 ± 0.3 (with k = 0.001 ± 0.001) which was fairly similar to the multilayer biphenyl value of 4.4 ± 0.4

In the previous work, the increase in fluorescence intensity was attributed to the percolation of cyclohexane into the biphenyl layer that caused the increase in the density of defects within the biphenyl adlayer.[18] Hence, the thicker the cyclohexane adlayer, the larger was the fluorescence intensity.[18]

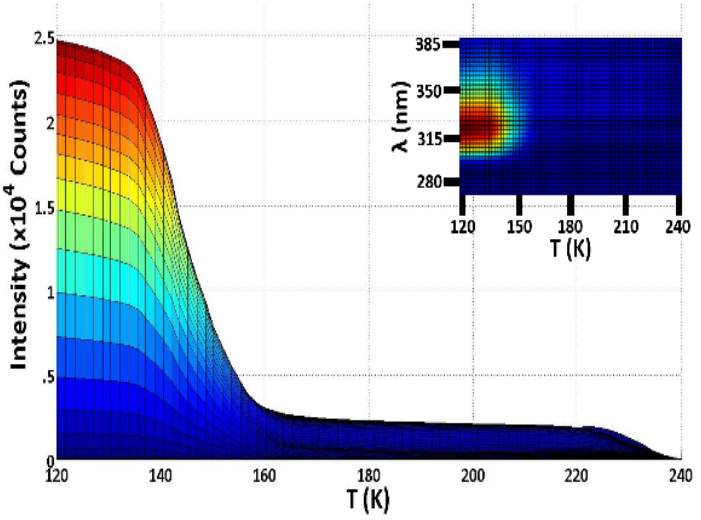


**Figure 4**. Wavelength-resolve TPD of methanol-biphenyl bilayer with $\Theta_{methanol}$ = 2 ML, $\Theta_{biphenyl}$ = 114 ML. Note the disorder-to-order transition that occurs at about 144 K with a concomittant red-shift in $\lambda_{max}$ and decrease in fluorescence intensity to about 10% of the initial intensity. Inset: top view.

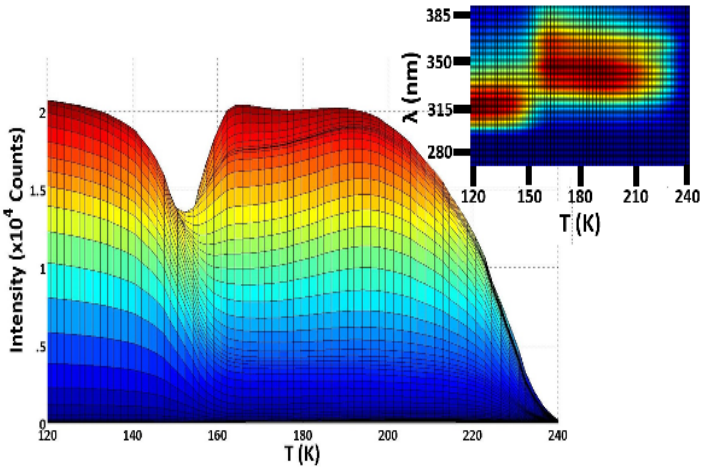


**Figure 5**. Wavelength-resolve TPD of cyclohexane-biphenyl bilayer with $\Theta_{cyclohexane}$ = 264 ML, $\Theta_{biphenyl}$ = 110 ML. The disorder-to-order transition occurs at 150 K with a concomittant red-shift in $\lambda_{max}$. Inset: top view.

The enhancement in fluorescence is plotted in Figure 6 where the fluorescence intensity subsequent to the disorder-to-order transition was normalized against the intensity at the beginning to of the TPD so that the slight differences in coverages could be taken into account. The scatter in the data was due in part to the fact that the formation of defect sites is probabilistic.

The hypothesis that cyclohexane increased the density of trap sites (defect) was supported by two observations: 1. If the cyclohexane was deposited on top of biphenyl, the enhancement in the fluorescence was not observed. Therefore percolation of the cyclohexane through the biphenyl layer was required to observe this increase in intensity. 2. The nucleation-crystallization kinetics of biphenyl was not as affected in terms of the n value and the range of temperature within which the transition occurred. Even though $T_p$ for cyclohexane is lower than the disorder-to-order transition temperature, the presence of cyclohexane was not effective until the biphenyl had undergone its disorder-to-order transition and at which time, defect sites within the ordered adlayer can be formed. The implication was that cyclohexane served to increase the density of defect sites, but did not induce the disorder-to-order transition.

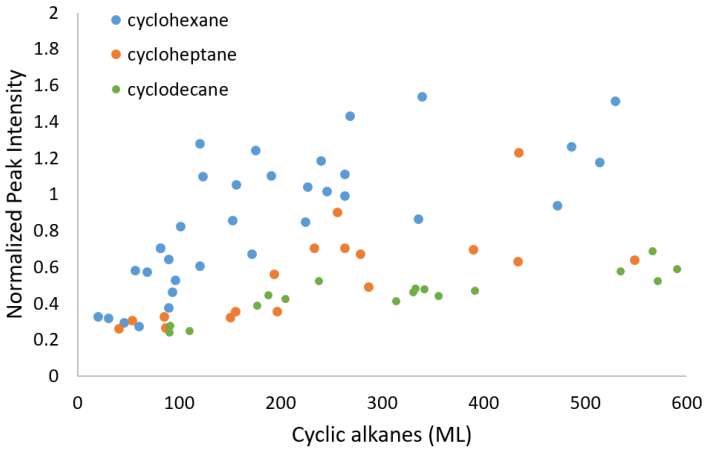


**Figure 6**. Plot of the peak of the fluorescence intensity due to the cycloalkane after the disorder-to-order transition normalized to intensity at the start of the TPD to account for the difference in biphenyl coverages for each point. Here, $\Theta_{biphenyl}$ was kept constant with 130 ± 30 ML

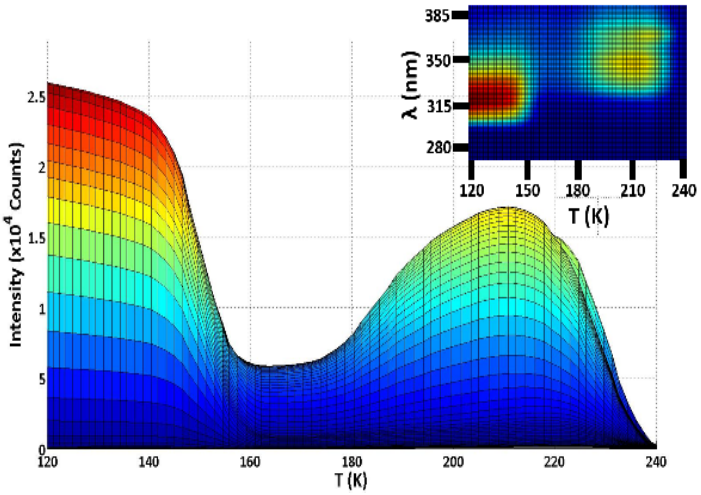


**Figure 7**. Wavelength-resolve TPD of cycloheptane-biphenyl bilayer with $\Theta_{cycloheptane}$ = 279 ML, $\Theta_{biphenyl}$ = 129 ML. The disorder-to-order transition occurs at 150 K with a concomitant red-shift in $\lambda_{max}$ . Inset: top view.

*Cycloheptane-Biphenyl Bilayer*

Cycloheptane desorbed at 159 K with an activation energy for desorption of 40.7 kJ/mol. Note that $T_p$ was the same temperature as the disorder-to-order transition of biphenyl. The cycloheptane adlayer had a slight effect on the disorder-to-order transition in biphenyl: the onset was at 142 K, ending at 158 K, and the mid-point temperature was 150 K, about the same as with cyclohexane. A representative wavelength-resolved TPD is shown in Figure 7.

The nucleation-crystallization kinetics analysis gave a n value of 3.7 ± 0.14 (with k = 0.002 ± 0.001), which led to the conclusion that the process was tending towards multilayer biphenyl behavior. These results were consistent with those for cyclohexane-biphenyl bilayers. The only difference was that cycloheptane was less effective in increasing the density of defect sites, as can be seen from Figure 6.

*Cyclodecane-Biphanyl Bilayer*

Cyclodecane desorbed at 200 K, and with that $T_p$, $E_a$ was calculated to be 51.8 kJ/mol. The wavelength-resolved TPD is shown in Figure 8, and in Figure 6, the normalized intensities as a func-

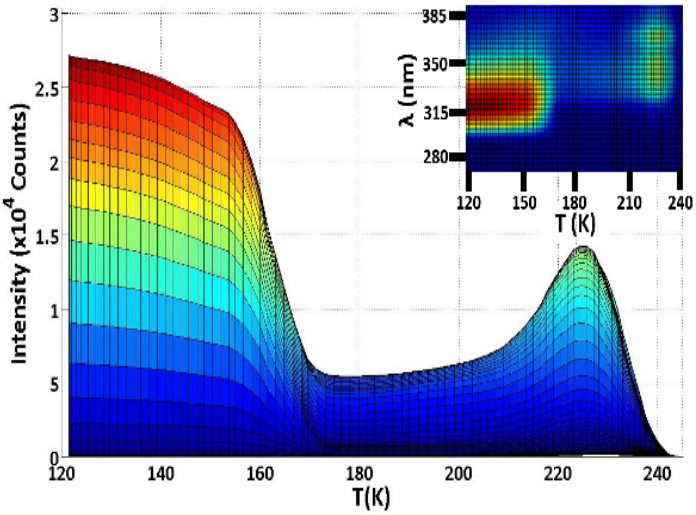


**Figure 8**. Wavelength-resolve TPD of cyclodecane-biphenyl bilayer with $\Theta_{cyclodecane}$ = 238 ML, $\Theta_{biphenyl}$ = 98 ML. The disorder-to-order transition occurs at 162 K with a concomitant red-shift in $\lambda_{max}$ . Inset: top view.

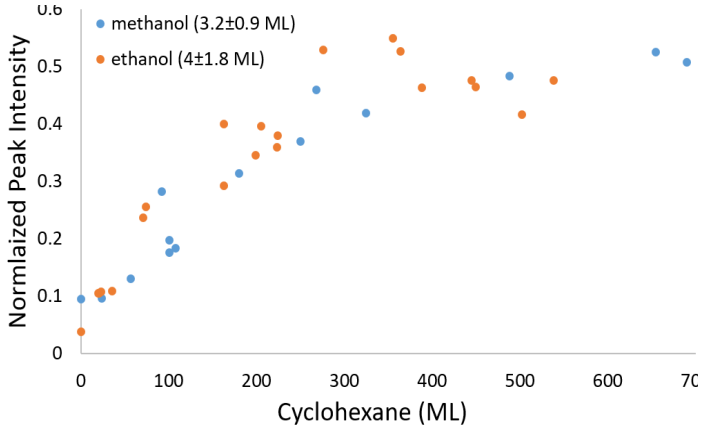


**Figure 9**. Plot of the peak of the fluorescence intensity after the disorder-to-order transition due to the cyclohexane's effect on biphenyl. In the trilayer ethanol and methanol was first layer deposited. The intensity was normaled against the start of the TPD to account for the difference in biphenyl coverages for each point. Here, $\Theta_{biphenyl}$ was kept constant with 120 ± 40 ML.

tion of cyclodecane coverage are given. The disorder-to-order transition began at 154 K, ended at 170 K with a mid-point of 162 K. The nucleation-crystallization analysis gave a n value of 4.6 ± 0.6 (with k = 0.1 ± 0.08), which was within error, identical to multilayer biphenyl. The cyclodecane data was consistent with the forementioned role cycloalkane played in producing defect sites. Interestingly, the transition temperature was raised with the larger alkyl ring. Notably, as seen from Figure 6, the effectiveness of the cycloalkane decreased with the size of the alkyl ring.

*Alcohol-Cyclohexane-Biphenyl Trilayer*

Given the two effects, causing the disorder-to-order transition at a lower temperature on one hand and on the other, causing an incease in the density of defect sites, which path would biphenyl take if *both* were simultaneously present? To determine the answer, a combination of alcohol-cycloalkane underlayers with a biphenyl overlayer was deposited. What was found was that the fluorescence intensity subsequent to the disorder-to-order transition was quenched. The results are plotted in Figure 9 for trilayers composed of methanol-cyclohexane-biphenyl and ethanol-cyclohexane-biphenyl. The intensities were taken at either 180 or 210 K, whichever temperature corresponded to the the maximum intensity. Note the difference in scale when compared to Figure 6.

What was immediately apparent was that for the smallest coverages of ethanol or methanol (~ 3-4 ML), the effectiveness of cyclohexane in producing defect sites was considerably muted. Hence the ethanol and methanol created nucleation sites more effectively than did the cyclohexane in creating defect sites.

*n-Alkane-Biphenyl Bilayer*

The $T_p$ for *n*-hexane was 144 K and the activation energy for desorption was calculated to be 36.9 kJ/mol.[15-17] Shown in Figure 10 is the wavelength-resolved TPD of the bilayer. The disorder-to-order transition started at 144 K, and ended at 166 K, with a mid-point temperature of 155 K. The wavelength-resolved TPD showed $\lambda_{max}$ peaks at 330 nm and 366 nm (Cf. Figure 10, right inset). The 330 nm peak increased in intensity at the disorder-to-order transition, and was assigned to the amorphously deposited biphenyl. This peak corresponded to the 315 nm peak in the multilayer biphenyl and represent a much more planar conformer (18º compared to 48º)[5] due to the interaction with *n*-hexane underlayer. After the transition, the 330 nm peak resolved into two peaks: one at 323 nm and another at 330 nm where the latter had been previously assigned to a vibrational progression[8]. At the transition, the intensity of the 366 nm peak increased to a maximum at 160 K (Cf Figure 10, right inset), and then decreased with the completion of the disorder-to-order transition. .

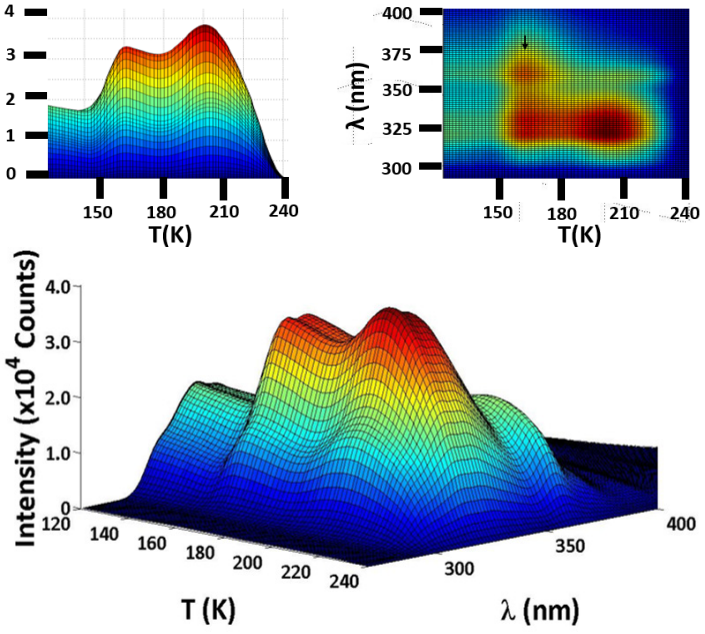


**Figure 10**. Wavelength-resolve TPD of *n*-hexane-biphenyl bilayer with $\Theta_{hexane}$= 183 ML, $\Theta_{biphenyl}$ = 112 ML. The disorder-to-order transition occurred at 155 K. Left inset: side view and right inset: top view where arrow points to the excimer with $\lambda_{maz}$ of 366 nm.

For *n*-heptane, the $T_p$ was 156 K, and $E_a$ was calculated to be 39.9 kJ/mol.[15-17] As shown in Figure 11, the wavelength-resolved TPD for the bilayer exhibited the disorder-to-order transition that began at 164 K, ended at 176 K, with a mid-point temperature of 169 K. The fluorescence spectra exhibit two $\lambda_{max}$s: one at 343 nm

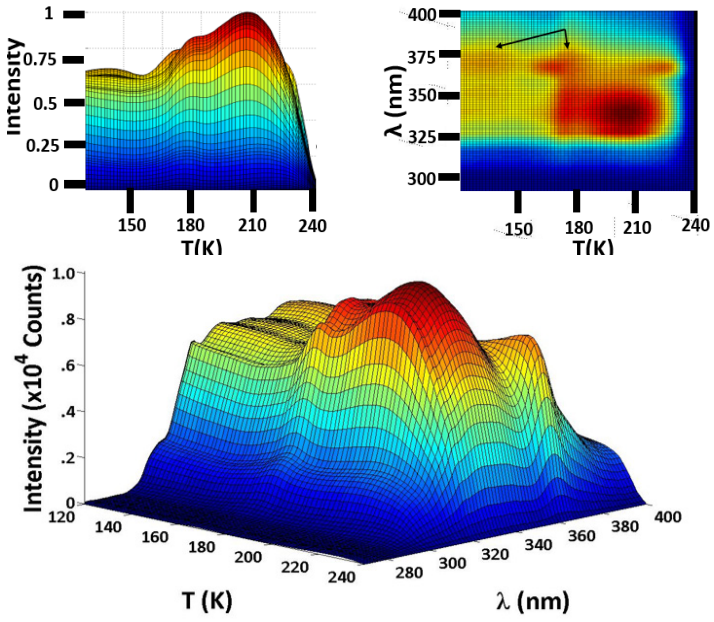


**Figure 11**. Wavelength-resolve TPD of *n*-heptane-biphenyl bilayer with $\Theta_{heptane}$= 247 ML, $\Theta_{biphenyl}$ = 116 ML. The disorder-to-order transition occurred at 169 K. Left inset: side view and right inset: top view where arrows point to the excimer with $\lambda_{maz}$ of 368 nm on the left and 367 nm on the right. The peak at 365 nm is Hg line.

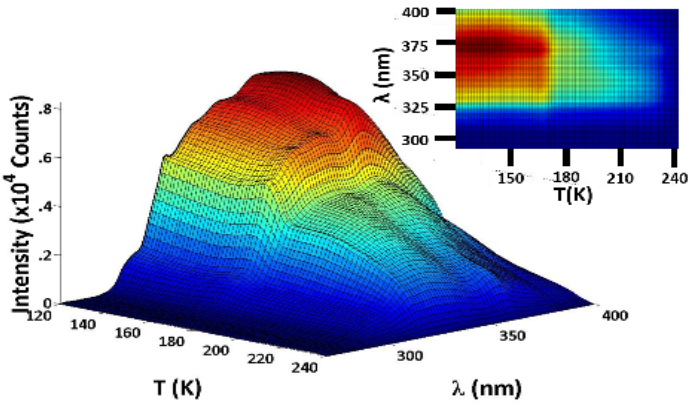


**Figure 12**. Wavelength-resolve TPD of *n*-heptane-biphenyl bilayer with $\Theta_{heptane}$= 32 ML, $\Theta_{biphenyl}$ = 134 ML. At these low coverages, the fluorescence emission is from the excimer only, with $\lambda_{maz}$ of 368 nm. The same were observed for low coverage underlayers of *n*-octane and *n*-nonane. Inset: top view.

and another at 368 nm. The former correspond to the planar conformer with a dihedral angle of ~1º,[5] and the latter was assigned to the excimer with planar dihedral angle (Cf. right inset to Figure 11). As shown in Figure 12, at low coverages of *n*-heptane in the bilayer, only the excimer fluorescence was observed. The intensity of the excimer decreased at the disorder-to-order transition. One possible reason for the emergence of excimer was that the *n*-heptane that composed the base layer line up parallel to each other due to London dispersion forces[20] and created a template upon which the biphenyl stacked up much like plates in a dish rack. In this proposed eclipsed form, the excimer can more easily form when a biphenyl molecule was electronically excited. For higher coverages, as with *n*-hexane, the fluorescence intensity increased at the disorder-to-order transition, susequent to which the fluorescence blue-shifted slightly to $\lambda_{max}$ =324 nm (dihedral angle of 29º).[5] This conformer was not as planar as it was for the multilayer.

For *n*-octane, the $T_p$ was 173 K and $E_a$ was 44.6 kJ/mol.[15-17] A representative wavelength-resolved TPD is shown in Figure 13. The disorder-to-order transition began at 179 K, ended at 196 K, and had a mid-point temperature of 186 K. With *n*-octane as the underlayer, $\lambda_{max}$s at 333 nm and 369 nm were observed. The 333 nm peak became very intense at the disorder-to-order transition and bifurcated to distinct peaks, one at 322 nm and the more intense peak at 333 nm due to vibrational progression[8]. The excimer peak at 369 nm, decreased in intensity with temperature, but at about 172 K until 180 K, the 4-nm blue-shifted excimer peak ($\lambda_{max}$~ 365 nm) emerged (indicated by arrow in left and right insets). Subtle molecular dynamics resulted in a temporal arrangement of *n*-octane to allow biphenyl molecules to retain the amorphous morphology and caused the excimer to form. As with *n*-heptane, low coverages of *n*-octane caused the formation of biphenyl excimer, almost identical to that shown in Figure 12.

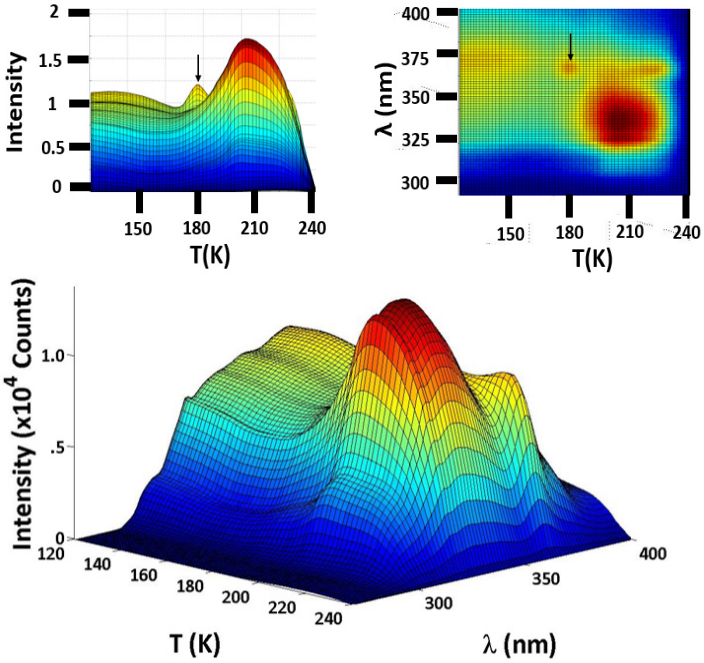


**Figure 13**. Wavelength-resolve TPD of *n*-octane-biphenyl bilayer with $\Theta_{octane}$ = 199 ML, $\Theta_{biphenyl}$ = 168 ML. The disorder-to-order transition occurred at 186 K. Left inset: side view. Arrow points to excimer at 365 nm. Right inset: top view where arrows point to the same excimer peak with $\lambda_{maz}$ of 365 nm as indicated on the left inset. Upon deposition of the bilayer, the excimer immediately formed with a $\lambda_{maz}$ of 369 nm as seen to the left of the excimer indicated by the arrow.

For *n*-nonane, $T_p$ at low coverages was measured at 181 K with a $E_a$ of 51.1 kJ/mol.[15-17] As seen in Figure 14 and the corresponding insets, the disorder-to-order transition for the bilayer began at 143 K, ended at 155 K, with a mid-point temperature of 148 K. For *n*-nonane as with *n*-heptane and *n*-octane, low coverage, 20 - 30 ML, the bilayer exhibited only excimer fluorescence such as that shown in Figure 12. As with the other alkanes, *n*-nonane as an underlayer caused biphenyl's ordered form to be less planar than the multilayer. Since the disorder-to-order transition was distinct as can be seen from the left inset of Figure 14, the Avrami values were determined. Here, n = 4.1 ± 0.1, which was within experimental error, the same as with the multilayer.

For *n*-decane, the $T_p$ was 198 K and $E_a$ was 51.1 kJ/mol.[15-17] The wavelength-resolved TPD is shown in Figure 15. The disorder-to-order transition began at 141 K, ended at 163 K and the midpoint was at 152 K. By this point in the series of aliphatic alkanes, entropically driven disorder exceeded the dispersion forces. Here, sufficient disorganization of the alkane caused biphenyl to become more like the multilayer. Hence most of the intensity came from one peak at 313 nm, which would correspond to a dihedral angle of 53º.[5] As the temperature was increased beyond the transition in a TPD experiment, *n*-decane caused the normal density of defect sites to increase as it percolated through the biphenyl on to desorption. This increased the intensities of the peaks at 322 nm and 331 nm. The 368 nm wavelength intensity was barely visible for *n*-decane as the underlayer (Cf. right inset, arrow, Figure 15). Since the disorder-to-order transition was clearly observed, the Avrami values could be calculated. These constants were n = 4.0 ± 0.2 and k = 0.004 ± 0.004. The n value was closely aligned to the multilayer.

In Figure 16, the fluorescence intensities after the disor-

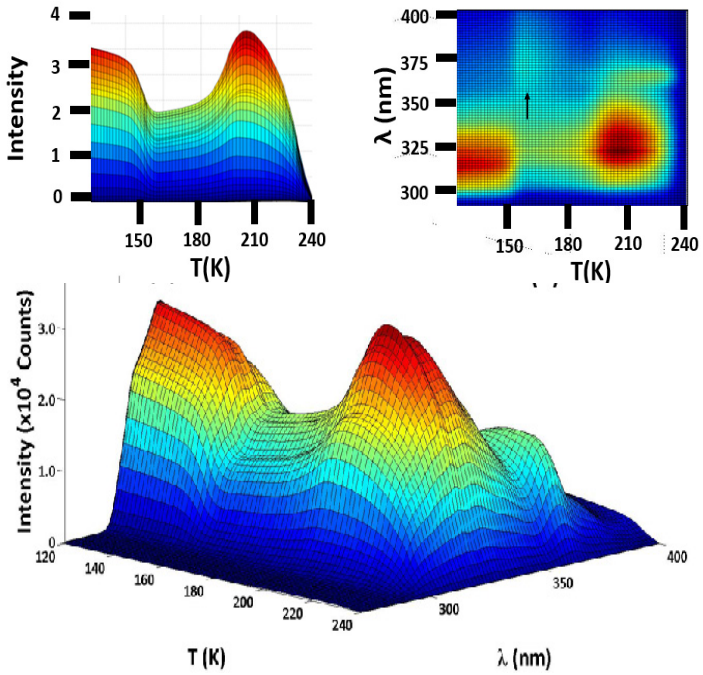


**Figure 14**. Wavelength-resolve TPD of *n*-nonane-biphenyl bilayer with $\Theta_{n\text{-}nonane}$ = 171 ML, $\Theta_{biphenyl}$ = 154 ML. The $\lambda_{max}$ initially was at 315 nm and then red shifted to 324 nm. Left inset: side view. Right inset: top view. Arrow points to the excimer. The peak at 365 nm is the Hg line.

der-to-order transition are plotted as a function of coverage of the *n*-alkane underlayer with a fixed coverage of biphenyl: 130 ± 50 ML. The intensities were normalized against the initial intensities to account for the run-to-run variation in biphenyl coverages. The maxima in the density of defect sites were observed at about 400 ML of *n*-alkane. Attempts will be made to model the interaction with a stoichiometric ratio of 4 molecules of alkane per biphenyl. Finally, all of the values referenced to in the text have been summarized in Table S-T. (See below).

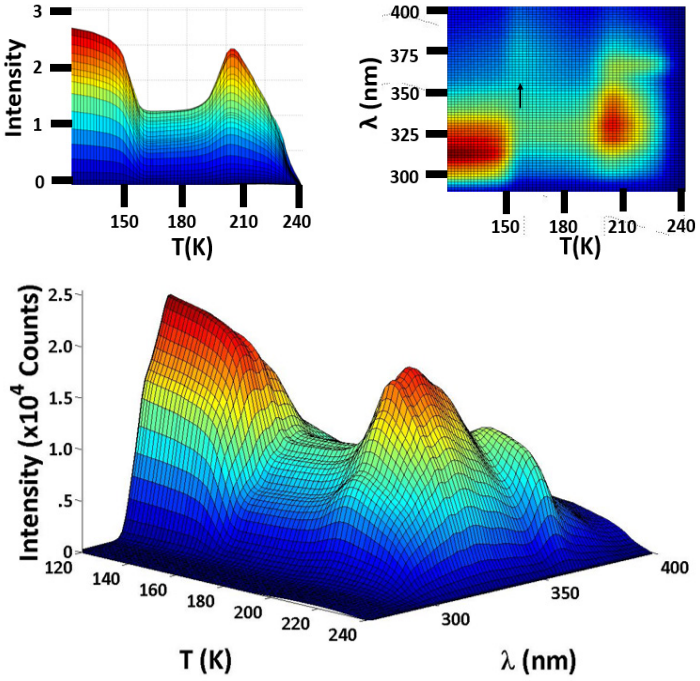


**Figure 15**. Wavelength-resolve TPD of *n*-decane-biphenyl bilayer with $\Theta_{decane}$ = 163 ML, $\Theta_{biphenyl}$ = 122 ML. The $\lambda_{max}$ initially was at 313 nm and then red shifted to 322 nm, with a vibrational progression at 331 nm. Left inset: side view. Right inset: top view. Arrow points to the excimer at 368 nm.

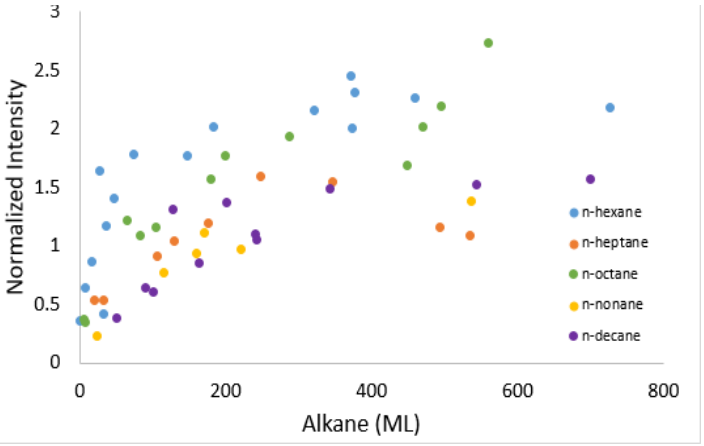


**Figure 16**. Normalized enhanced biphenyl fluorescence intensities as a function of *n*-alkane coverage. Plot of the peak of the fluorescence intensity after the disorder-to-order transition due to the *n*-alkane's effect on biphenyl. The intensity was normaled against the start of the TPD to account for the slight difference in biphenyl coverages for each point. Here, the biphenyl coverage was kept constant at $\Theta_{biphenyl}$ = 130 ± 50 ML.

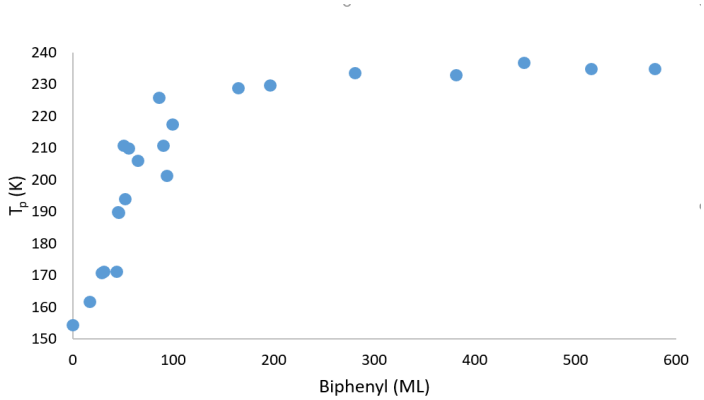


**Figure S-1**. Evidence of cluster formation for molecules capable of H-bonding. Hold down effect of $H_2O$ as an underlayer with biphenyl as overlayer. $T_p$'s for multilayer $H_2O$ and biphenyl were 154.3 K and 227.2 K, respectively. $\Theta_{H_2O}$ was kept constant at 50 ± 20 ML.

**Table S-T**. Summary of referenced data.

| Compound | $T_p$ (K) | $E_a$ (kJ/mol) | Avrami n | Avrami k | Excimer | Transition (K) | Hold Down (K) | Initial λ (nm) (°)[5] | Final λ (nm) (°)[5] |
|---|---|---|---|---|---|---|---|---|---|
| biphenyl | 227 | 58.9 | 4.4 ± 0.4 | 0.1 ± 0.12 | no | 158 | 0 | 315 (48°) | 337 (8°) |
| water | 144 | 36.9 | 4.5 ± 0.1 | 0.03 ± 0.02 | no | 157 | 73 | 318 (41°) | 340 (4°) |
| methanol | 139 | 35.6 | 3.1 ± 0.3 | 0.0008 ± 0.0006 | no | 144 | 11 ± 3 | 313 (53°) | 333 (8°) |
| ethanol | 148 | 37.8 | 2.6 ± 1.2 | 0.04 ± 0.03 | no | 150 | 11 ± 5 | 316 (46°) | 337 (8°) |
| 1-propanol | 159 | 40.8 | 3 ± 1 | 0.003 ± 0.01 | no | 148 | 1 | 315 (48°) | 345 (~0°) |
| 1-butanol | 178 | 45.8 | 3.5 ± 4 | 0.007 ± 0.01 | no | 152 | 2.1 | 315.5 (47°) | 345 (~0°) |
| 1-pentanol | 183 | 47.3 | 4.1 ± 4 | 0.01 ± 0.01 | no | 155 | 1 | 316 (46°) | 343 (1°) |
| 1-hexanol | 193 | 49.9 | 5.4 ± 5 | 0.006 ± 0.01 | no | 158 | 1 | 316 (46°) | 339 (6°) |
| cyclohexane | 138 | 35.2 | 4.0 ± 0.3 | 0.001 ± 0.001 | weak | 148 | 17.2 ± 0.8 | 316 (46°) | 346 (~0°) |
| cycloheptane | 159 | 40.7 | 3.7 ± 0.2 | 0.002 ± 0.001 | no | 150 | 21 ± 2 | 317 (44°) | 342 (2°) |
| cyclodecane | 200 | 51.8 | 4.6 ± 0.6 | 0.01 ± 0.08 | no | 162 | 20 ± 6 | 313 (53°) | 340 (4°) |
| *n*-hexane | 144 | 36.9 | N/A | N/A | weak | 155 | 6 ± 3 | 330 (18°),366 (0°) | 323 (31°) |
| *n*-heptane | 156 | 39.9 | N/A | N/A | strong | 169 | 12 ± 2 | 343 (1°), 368 (0°) | 324 (29°) |
| *n*-octane | 173 | 44.6 | N/A | N/A | strong | 186 | 8 ± 4 | 333 (14° ),369 (0°) | 322 (33°) |
| *n*-nonane | 181 | 46.5 | 4.1±0.1 | 0.00029±0.0009 | strong | 148 | 9 ± 3 | 315 (48°) | 324 (29°) |
| *n*-decane | 198 | 51.1 | 4.0 ± 0.2 | 0.004 ± 0.004 | weak | 163 | 3 ± 2 | 313 (53°) | 322 (33°) |

In summary, the key points are enumerated here: 1. The discovery that the mechanism for the disorder-to-order transition was nucleation-crystallization induction of vapor deposited biphenyl by hydrogen-bonded clusters of small chained alcohols or water might be more generally applicable to other organic systems. The Avrami n values was a good indicator of the effect of alcohol by forming nucleation sites. (Cf Table S-T 4th column). 2. The results here suggest that molecules of comparable sized cyclic and *n*-aliphatic hydrocarbons might be used to increase the density of defect sites in the fluorophore overlayer. In this way, fluorescence could be used to probe the surface dynamics of other vapor deposited organic films which otherwise might be too dim to study directly. 3. The loosely defined term, 'hold down' effect for ethanol and methanol was evidence of molecular cluster. (Cf. Table S-T, 3rd column from right). The large hold down effect for the cyclic alkanes might be surprising. Some of the *n*-alkanes also exhibited a surprisedly strong hold down effect, particularly those that gave rise to excimer formation. This was taken as evidence for the presence of dispersion forces. 4. Upon deposition, the hydrocarbon underlayer caused biphenyl to deposit in highly planar conformers compared to the multilayer. In the case of *n*-heptane, *n*-octane, and *n*-nonane, the morphology of the deposited underlayer allowed biphenyl molecules to be in such close proximity that solely excimers were detected. 5. With the alkane underlayer, subsequent to the disorder-to-order transition, the dihedral angle was twisted at angle of 31º ±2 compared to 8º for the multilayer. (Cf. Table S-T, last column). 6. Finally, the variation in the dihedral angles of the ordered form was an indicator of the degree to which biphenyl accommodated the variation in the morphology of the underlayer. (Cf. Table S-T, last column).

**Acknowledgement**

S.T.W. and I.Z.S. gratefully acknowledge the John Stauffer Charitable Trust for funding the student stipends for summer research.

**References**

1 A. Almenningen, O. Bastiansen, L. Fernholt, B.N. Cyvin, S.J. Cyvin and S. Samdal. *J. Mol. Str*uct., **1985**, 128, 59-76.
2. G.P. Charbonneau and Y. Delugeard. *Acta Crystallographica B*, **1976**, 32, 1420-1423.
3. M.K. Condie, Z.E. Moreau and A.M. Nishimura. *J. Undergrad. Chem. Res*., **2019**, 18, 15-18.
4. B.D. Fonda, M.K. Condi, Z.E. Moreau, Z.I. Shih, B. Dionisio, A. Fitts, L. Foltz, K. Nili and A.M. Nishimura. *J. Phys. Chem. C*., **2019**, 123, 26185-26190.
5. Nicole M. Bond and A.M. Nishimura, *JUCR*, **2022,** 21, 84-92.
6. Karli R. Holman, Xianzhang Geng, K.A. Martin and A.M. Nishimura, *J. Lumin.*, **2017**, *181*, 19-24.
7. Blake D. Fonda, Jonathan B. Cleek, K.A. Martin and A.M. Nishimura, *JUCR*, **2017**, 16, 85-88.
8. Jonathan B. Cleek, Blake D. Fonda, K.A. Martin and A.M. Nishimura, *JUCR*, **2017**, 16, 110-114.
9. Melvin Avrami, *J. Chem. Ph*ys. **1939**, 7, 1103-1112; **1940**, 8, 212-224.
10. N.J. Tro, A.M. Nishimura, D.R. Haynes and S.M. George, *Surface Science Lett.* **1989**, 207, L961-L970.
11. I.M. Rosbrugh, D.W. West, L.E. Pfeifer, N.M. Cook, D.M. Licata, K.A. Martin and A.M. Nishimura, *Surface Science Lett.* **2000,** L248-L254.
12. Timothy LeDoux, Jonathan Brigham, K.A. Martin and A.M. Nishimura, *JUCR*, **2003,** 3, 35-39.
13. M.A. Evans, D.R. Hoss, K.E. Howard, A.D. Louie, A.J. Bishop, K.A. Martin and A.M. Nishimura, *Thin Solid Films*, **2006**, 515, 1370-1376.
14. J.S. Brigham, A.J. Bishop, T.S. LeDoux, J.M. Rea, K.A. Martin and A.M. Nishimura, *JUCR*, **2004**, 4, 169-171.
15 P.A. Redhead. *Vacuum,* **1962**, 12, 203-211.
16. F.M. Lord and J.S. Kittelberger. *Surf. Sci*., **1974**, 43, 173-182.
17. D.A. King. *Surf. Sci*., **1975**, 47, 384-402.
18. Samie Watanabe, Isaac Song, Nicole Bond, John Baker, Mariyan Popov and A.M. Nishimura. *JUCR*, 2023, 22, 66-68.
19. Marissa K. Condie, Christian Kim, Zackery E. Moreau, Bryan Dionisio, Katie Nili, Jacob Francis, Cassidy Tran, Sean Nakaoka and A.M. Nishimura, *JUCR*, **2020**, 18, 14-17.
20. Frederick M. Fowkes, *J. Phys. Chem*., **1980**, 84, 510-512.